Updating Solutions of the Rational Function Model Using Additional Control Information

Yong Hu and C. Vincent Tao

Abstract

The rational function model (RFM) is a sensor model that allows users to perform ortho-rectification and 3D feature extraction from imagery without knowledge of the physical sensor model. It is a fact that the RFM is determined by the vendor using a proprietary physical sensor model. The accuracy of the RFM solutions is dependent on the availability and the usage of ground control points (GCPs). In order to obtain a more accurate RFM solution, the user may be asked to supply GCPs to the data vendor. However, control information may not be available at the time of data processing or cannot be supplied due to some reasons (e.g., politics or confidentiality). This paper addresses a means to update or improve the existing RFM solutions when additional GCPs are available, without knowing the physical sensor model. From a linear estimation perspective, the above issue can be tackled using a phased estimation theory. In this paper, two methods are proposed: a batch iterative least-squares (BILS) method and an incremental discrete Kalman filtering (IDKF) method. Detailed descriptions of both methods are given. The feasibility of these two methods is validated and their performances are evaluated. Some results concerning the updating of Ikonos imagery are also discussed.

Introduction

A rational function is a function that can be represented as the quotient of two polynomials. Mathematically speaking, all polynomials are rational functions (Newman, 1978). The rational function model (RFM) in this context is a sensor model representing the imaging geometry between the object space and the image space.

The RFM has gained considerable interest recently mainly due to the fact that Space Imaging Inc. (Thornton, Colorado) has adopted the RFM as a replacement sensor model for image exploitation. The RFM is provided to end users for photogrammetric processing instead of the Ikonos physical sensor model. Such a strategy can serve two purposes. On the one hand, the use of an RFM may help keep information about the sensor confidential because it is difficult to derive the physical sensor parameters from the RFM. On the other hand, rational function models facilitate the exploitation of high-resolution satellite imagery by end users. With the RFM provided, users and developers are able to perform photogrammetric processing such as ortho-rectification, 3D feature extraction, and DEM generation from imagery without knowing the complex physical sensor model (Tao and Hu, 2001a; Tao and Hu, 2001b). Tests have shown that the RFM can achieve a very high fitting accuracy to the physical sensor model and is capable of replacing the rigorous sensor models for photogrammetric restitution (Madani, 1999; Dowman and Dolloff, 2000; Yang, 2000; Tao and Hu, 2001c). It was reported in Grodecki (2001) that the Ikonos rational model differs by no more than 0.04 pixel from the physical sensor model, with the RMS error below 0.01 pixel.

The RFM solutions are determined by the data vendor using a proprietary physical sensor model. The accuracy of the RFM solutions is dependent on the availability and the usage of the GCPs. If accurate RFM solutions are required, GCPs are needed and are incorporated into the RFM solution process. In this case, the user may be asked to supply the GCPs to the data vendor. However, the GCPs may not be available at the time of processing or cannot be supplied due to some reasons (e.g., politics or confidentiality).

If additional GCPs are available, one may ask if it is possible to update or improve the existing RFM solutions (provided, for example, by the vendor). In this paper, we present an approach to update and/or improve the existing RFM solutions when additional GCPs are available, given that the physical sensor model is unknown. In the next section, we briefly describe the RFM by introducing a least-squares solution as well as two computation scenarios for RFM determination. In the following section, we present two methods for updating the initial RFM solution, namely, a batch iterative least-squares (BILS) method and an incremental discrete Kalman filtering (IDKF) method using additional GCPs. Finally, we show the results computed by both the BILS and IDKF methods to demonstrate the feasibility and the performance of each method. An aerial photograph and an Ikonos stereo pair were used in the experiments. The left and right images of the Ikonos stereo pair were updated and three-dimensional reconstruction was done to check the possibility to update the rational function coefficients (RFCs) without further information about their covariance.

Solutions to the Rational Function Model

Direct and Iterative Least-Squares Solutions

The RFM uses a ratio of two polynomial functions of ground coordinates to compute the row image coordinate, and a similar ratio to compute the column image coordinate. The two image coordinates (row and column) and three ground coordinates (e.g., latitude, longitude, and height) are each offset and scaled to fit the range from −1.0 to 1.0 over an image or an image sec-

Y. Hu is with the Department of Geomatics Engineering, The University of Calgary, 2500 University Dr. NW, Calgary, Alberta T2N 1N4 Canada (yhu@ucalgary.ca).

C.V. Tao is with the Geospatial Information and Communication Technology (Geo-ICT) Lab, Department of Earth and Atmospheric Science, York University, 4700 Keele Street, Toronto, Ontario M3J 1P3, Canada (tao@yorku.ca)

Photogrammetric Engineering & Remote Sensing
Vol. 68, No. 7, July 2002, pp. 715–723.

0099-1112/02/6807–715$3.00/0

tion. A detailed description of this normalization process can be found in OpenGIS Consortium (1999). For the ground-to-image transformation, the defined ratios of polynomials have the form (Greve, 1992)

$$r_n = \frac{\sum_{i=0}^{m1}\sum_{j=0}^{m2}\sum_{k=0}^{m3} a_{ijk}X_n^iY_n^jZ_n^k}{\sum_{i=0}^{n1}\sum_{j=0}^{n2}\sum_{k=0}^{n3} b_{ijk}X_n^iY_n^jZ_n^k}$$
$$c_n = \frac{\sum_{i=0}^{m1}\sum_{j=0}^{m2}\sum_{k=0}^{m3} c_{ijk}X_n^iY_n^jZ_n^k}{\sum_{i=0}^{n1}\sum_{j=0}^{n2}\sum_{k=0}^{n3} d_{ijk}X_n^iY_n^jZ_n^k} \quad (1)$$

where r_n and c_n are the normalized row and column indices, respectively, of pixels in the image; X_n, Y_n, and Y_n are normalized coordinate values of object points in ground object space; and a_{ijk}, b_{ijk}, c_{ijk}, and d_{ijk} are polynomial coefficients called *rational function coefficients (RFCs)*. The maximum power of each ground coordinate ($m1$, $m2$, $m3$, $n1$, $n2$, and $n3$) is typically limited to 3; and the total power of all ground coordinates is also limited to 3. The unknown RFCs can be solved for by using a linear least-squares method. The linearized form of Equation 1 with respect to the RFCs can be written as

$$v_r = \left[\frac{1}{B}\frac{Z}{B}\frac{Y}{B}\frac{X}{B}\cdots\frac{Y^3}{B}\frac{X^3}{B} - \frac{rZ}{B} - \frac{rY}{B}\cdots - \frac{rY^3}{B} - \frac{rX^3}{B}\right]\cdot\mathbf{J} - \frac{r}{B} \quad (2a)$$

$$v_c = \left[\frac{1}{D}\frac{Z}{D}\frac{Y}{D}\frac{X}{D}\cdots\frac{Y^3}{D}\frac{X^3}{D} - \frac{cZ}{D} - \frac{cY}{D}\cdots - \frac{cY^3}{D} - \frac{cX^3}{D}\right]\cdot\mathbf{K} - \frac{c}{D} \quad (2b)$$

or

$$v_r' = Bv_r = [1\ Z\ Y\ X\cdots\ Y^3\ X^3\ -rZ\ -rY\cdots\ -rY^3\ -rX^3]\cdot\mathbf{J} - r \quad (3a)$$

$$v_c' = Dv_c = [1\ Z\ Y\ X\cdots\ Y^3\ X^3\ -cZ\ -cY\cdots\ -cY^3\ -cX^3]\cdot\mathbf{K} - c \quad (3b)$$

where

$$B = (1\ Z\ Y\ X\cdots\ Y^3\ X^3)\cdot(1\ b_1\cdots\ b_{19})^{\mathrm{T}}$$
$$\mathbf{J} = (a_0\ a_1\cdots\ a_{19}\ b_1\ b_2\cdots\ b_{19})^{\mathrm{T}}$$
$$D = (1\ Z\ Y\ X\cdots\ Y^3\ X^3)\cdot(1\ d_1\cdots\ d_{19})^{\mathrm{T}}$$
$$\mathbf{K} = (c_0\ c_1\cdots\ c_{19}\ d_1\ d_2\cdots\ d_{19})^{\mathrm{T}}$$

Given n GCPs, the observation error equations can be formed as

$$\begin{bmatrix}\mathbf{V}_r\\ \mathbf{V}_c\end{bmatrix} = \left[\begin{array}{c|c}\mathbf{W}_r & \mathbf{O}\\ \hline \mathbf{O} & \mathbf{W}_c\end{array}\right]\cdot\left[\begin{array}{c|c}\mathbf{M} & \mathbf{O}\\ \hline \mathbf{O} & \mathbf{N}\end{array}\right]\cdot\begin{bmatrix}\mathbf{J}\\ \mathbf{K}\end{bmatrix} - \left[\begin{array}{c|c}\mathbf{W}_r & \mathbf{O}\\ \hline \mathbf{O} & \mathbf{W}_c\end{array}\right]\cdot\begin{bmatrix}\mathbf{R}\\ \mathbf{C}\end{bmatrix} \quad (4a)$$

$$\mathbf{V} = \mathbf{WT}\,\mathbf{I} - \mathbf{WG} \quad (4b)$$

where

$$\mathbf{M} = \begin{bmatrix}1 & Z_1 & \cdots & X_1^3 & -r_1Z_1 & \cdots & -r_1X_1^3\\ 1 & Z_2 & \cdots & X_2^3 & -r_2Z_2 & \cdots & -r_2X_2^3\\ \vdots & \vdots & \ddots & \vdots & \vdots & \ddots & \vdots\\ 1 & Z_n & \cdots & X_n^3 & -r_nZ_n & \cdots & -r_nX_n^3\end{bmatrix},$$

$$\mathbf{N} = \begin{bmatrix}1 & Z_1 & \cdots & X_1^3 & -c_1Z_1 & \cdots & -c_1X_1^3\\ 1 & Z_2 & \cdots & X_2^3 & -c_2Z_2 & \cdots & -c_2X_2^3\\ \vdots & \vdots & \ddots & \vdots & \vdots & \ddots & \vdots\\ 1 & Z_n & \cdots & X_n^3 & -c_nZ_n & \cdots & -c_nX_n^3\end{bmatrix},$$

$$\mathbf{R} = \begin{bmatrix}r_1\\ r_2\\ \vdots\\ r_n\end{bmatrix},\ \mathbf{C} = \begin{bmatrix}c_1\\ c_2\\ \vdots\\ c_n\end{bmatrix}$$

and $\mathbf{W}$ can be considered as the weight matrix for the residuals at the left side of Equation 3: i.e.,

$$\mathbf{W} = \begin{bmatrix}\mathbf{W}_r & 0\\ 0 & \mathbf{W}_c\end{bmatrix},\ \mathbf{W}_r = \begin{bmatrix}\frac{1}{B_1} & 0 & \cdots & 0\\ 0 & \frac{1}{B_2} & 0 & \vdots\\ \vdots & 0 & \ddots & 0\\ 0 & \cdots & 0 & \frac{1}{B_n}\end{bmatrix},$$

$$\mathbf{W}_c = \begin{bmatrix}\frac{1}{D_1} & 0 & \cdots & 0\\ 0 & \frac{1}{D_2} & 0 & \vdots\\ \vdots & 0 & \ddots & 0\\ 0 & \cdots & 0 & \frac{1}{D_n}\end{bmatrix}.$$

The normal equation is then

$$\mathbf{T}^{\mathrm{T}}\mathbf{W}^2\mathbf{TI} - \mathbf{T}^{\mathrm{T}}\mathbf{W}^2\mathbf{G} = 0. \quad (5)$$

There are two solutions to Equation 5, the direct solution and the iterative solution. The direct solution to the RFCs is given by setting $\mathbf{W}$ to be the identity matrix. In this case, the normal Equation 5 can be solved using a standard least-squares method. As for the iterative solution, the initial value $\mathbf{I}^{(0)}$ of the coefficients can first be solved using the direct method; then $\mathbf{W}^{(j)}$ and $\mathbf{I}^{(j)}$ can be calculated by solving the normal equation iteratively until some termination condition is satisfied. The details regarding the two solutions as well as their comparative study results can be found in Tao and Hu (2001c; 2001d).

Assuming that the covariance of error, $\mathbf{R}_G$, associated with image pixel coordinates is known, the covariance matrix $\mathbf{P}$ associated with the coefficients $\mathbf{I}$ can be computed by (Krakiwsky, 1990)

$$\mathbf{P} = [\mathbf{T}^{\mathrm{T}}\,\mathbf{R}_G^{-1}\mathbf{T}]^{-1}. \quad (6)$$

The covariance of GCPs in the image after the solution is then given by

$$\mathbf{C} = \mathbf{TPT}^{\mathrm{T}} + \mathbf{R}_G \quad (7)$$

where $\mathbf{TPT}^{\mathrm{T}}$ is introduced by the ground-to-image transformation of the RFM (Equation 1).

Determination of RFCs

The RFCs can be solved for with or without knowing the physical sensor model. With the known physical sensor model, an

image grid covering the full extent of the image can be established and its corresponding 3D object grid can be generated, with each grid point's coordinates calculated from its corresponding image point using the physical sensor model. Then the RFCs can be estimated using a direct least-squares solution with an input of the object grid points (X, Y, Z) and the corresponding image grid points (r, c). Tests have shown that the RFM determined using this approach can achieve a very high fitting accuracy to its corresponding physical sensor model, and, thus, it can be used as a replacement sensor model for photogrammetric restitution (Paderes and Mikhail, 1989; Madani, 1999; Yang, 2000; Tao and Hu, 2001c). It is a fact that, in this approach, no actual terrain information is required. The RFM performs as a fitting function between the image grid and the object grid. Therefore, if the RFM is used for ortho-rectification and 3D reconstruction, the achievable accuracy is subject to the physical sensor model used. We call this approach the terrain-independent solution to the RFM (Tao and Hu, 2001c).

Without knowing the physical sensor model, the 3D object grid cannot be generated. Therefore, a sufficient number of GCPs on the terrain surface have to be collected in a conventional manner (e.g., from maps or a DEM). The iterative least-squares solution with regularization is then used to solve for the RFCs. In this case, the solution is highly dependent on the actual terrain relief, the number of GCPs, and their distribution across the scene. We call this approach the terrain-dependent solution to the RFM. Unless a large number of densely distributed GCPs is available, this approach may not provide a sufficiently accurate and robust solution to the RFM (Toutin and Cheng, 2000; Tao and Hu, 2001c). Because the RFM that is solved using this approach has no link to the physical sensor, it cannot be used as a replacement sensor model. However, this approach can be used as a general tool for image registration with some advantages and unique characteristics compared to the regular polynomial based methods (Tao and Hu, 2001d).

Update of Solutions Using Additional GCPs

Two methods are proposed to update the RFM solutions (i.e., the RFC values), given no knowledge of the physical sensor model. Assuming that the values of the RFCs have been pre-determined–when both the original and the additional GCPs are available–the values of the RFCs can again be solved for using the batch iterative least-squares method. When only the additional GCPs are available, an incremental method can be applied. Here, the original GCPs refer to those used to compute the initial RFC values, whereas the additional GCPs are independently collected and are not used to solve for the initial RFC values.

Batch Iterative Least-Squares (BILS) Method

For this method, we use both the original and the new control points to re-calculate the RFCs in a batch manner. This can be fulfilled by simply incorporating all the control points into the normal equation (Equation 5) with appropriate weighting for the original and new control points. In fact, this method may be used by the vendor when both the original and the new GCPs are known.

Incremental Discrete Kalman Filtering (IDKF) Method

For this method, the existing solution computed using the original GCPs can be updated in an incremental manner, provided that both the RFCs $\mathbf{I}$ and the covariance matrix $\mathbf{P}$ (Equation 6) associated with them are known. This method can be used by end-users to update the existing RFM solutions (provided by the vendor) using the new GCPs, which may be collected from time to time.

Process Model

Because the true values of the RFCs are constant with respect to time, this static process with the linear measurement of the process can be modeled in the form

$$\mathbf{I}_{k+1} = \mathbf{I}_k + \mathbf{w}_k \tag{8}$$

$$\mathbf{G}_k = \mathbf{T}_k\mathbf{I}_k - \mathbf{V}_k = \mathbf{T}_k\mathbf{I}_k + \mathbf{v}_k \tag{9}$$

where $\mathbf{w}_k$ is the process noise vector assumed to be a white sequence with known process noise covariance matrix $\mathbf{Q}_k$, and $\mathbf{v}_k$ is the measurement error vector assumed to be a white sequence with known covariance structure $\mathbf{R}_k$ that is associated with the image pixel coordinates of new GCPs. The vectors $\mathbf{w}_k$ and $\mathbf{v}_k$ are assumed independent of each other. In practice, $\mathbf{R}_k$ is usually determined when collecting new GCPs, while $\mathbf{Q}_k$ is usually determined on the basis of experience and trial. Although the true values of the RFCs do not change from step to step, assuming a non-zero value for $\mathbf{Q}_k$ usually allows for more flexibility in tuning the RFCs as demonstrated in the experiments.

Incremental Updating by Discrete Kalman Filtering

To update the initial solution, the static process (Equation 8) with linearized measurements (Equation 9) can be solved for each group of new control points using an incremental technique based on the discrete Kalman filter (Brown and Hwang, 1997) or sequential least squares (Krakiwsky, 1990). The Kalman filter is usually applied to complicated temporal problems. Because the new GCPs may be available in a serial manner, the Kalman filter is applied to a spatial problem here due to its recursive nature.

(1) Predicate the *a priori* estimate and its covariance matrix,

$$\mathbf{I}_k^- = \mathbf{I}_{k-1},$$

$$\mathbf{P}_k^- = \mathbf{P}_{k-1} + \mathbf{Q}_{k-1}$$

where the "super minus" indicates that this is the estimate prior to assimilating the new measurements.

(2) Compute the Kalman gain

$$\mathbf{K}_k = \mathbf{P}_k^-\mathbf{T}_k^{\mathrm{T}}\left[\mathbf{T}_k\mathbf{P}_k^-\mathbf{T}_k^{\mathrm{T}} + \mathbf{R}_k\right]^{-1}$$

(3) Update the *a priori* estimate $\mathbf{I}_k^-$ by adding weighted residuals from the new measurements

$$\mathbf{I}_k = \mathbf{I}_k^- + \mathbf{K}_k\mathbf{v}_k,\ \mathbf{v}_k = \mathbf{G}_k - \mathbf{T}_k\mathbf{I}_k^-$$

(4) Compute the covariance for the updated estimate $\mathbf{I}_k$

$$\mathbf{P}_k = (\mathbf{E} - \mathbf{K}_k\mathbf{T}_k)\mathbf{P}_k^-$$

(5) Compute the covariance of error for new GCPs

$$\mathbf{C}_k = \mathbf{T}_k\mathbf{P}_k\mathbf{T}_k^{\mathrm{T}} + \mathbf{R}_k \tag{10}$$

The RFC solution can be updated completely by assimilating all of the new control points, thus running Steps (2) to (5) only once. Alternatively, the new control points can be broken into smaller groups, thereby requiring Steps (2) to (5) to be repeated for each group of new control points. It can be found in this incremental method that the covariance matrix associated with the RFCs of the initial solution is important for controlling the system sensitivity to the new GCPs, and for obtaining correct covariances for the new GCPs.

Experimental Results and Evaluation

Test Data Sets

Aerial Photograph Data

The test data were provided by Intermap Technologies Corp., Calgary, Canada. The digitized image (from an aerial photograph) with a 1-meter ground resolution and a DEM with a 2.5-meter ground resolution were used to collect control points.

The DEM was acquired by Intermap's STAR-3i airborne InSAR system in the Morrison, Colorado region. First, the aerial image was ortho-rectified using its collinearity equations and was resampled to a ground resolution of 2.5 meters so that it matched the DEM of 2.5 meters ground resolution. Then, a set of 50 GCPs well-distributed over the test region was collected from the ortho-rectified aerial image and the corresponding DEM. The measurements in the image are considered to be independent and have an error of zero mean with a standard deviation of 0.75 pixels in the original digitized image. The elevation of the selected GCPs varies from 1657.84 meters to 2059.39 meters. In the experiment, this set of 50 GCPs was used to compute the initial values of the RFCs. An independent set of 49 points was collected from the original ortho-rectified aerial image (with a 1-meter ground resolution) to serve as additional control points and check points. The standard deviation of image measurements is assumed to be 0.30 pixels in the image. Figure 1 provides a 3D view of the distribution of the 50 GCPs (marked by dot "•"), and 49 additional points (marked by cross "+").

Ikonos Stereo Images

The data were collected in a power development region in southern Ontario, Canada. An Ikonos stereo pair was acquired by Space Imaging on 12 July 2001. Both panchromatic 11-bit images were geometrically corrected to the *standard* level with a ground pixel size of 1 meter. Each image was supplied together with a set of RFCs and normalization parameters (i.e., offsets and scales), which were determined by the terrain-independent approach. The physical Ikonos sensor model was derived from the satellite ephemeris and attitude without using GCPs. The specified horizontal accuracy of standard Ikonos stereo products is 25 m CE90 (Grodecki and Dial, 2001).

We collected 28 ground points from the Canadian Geospatial Data Infrastructure (CGDI) Data Alignment Layer in the overlapped area of the stereo pair. The CGDI Data Alignment Layer (CDAL) data set consists of many feature points derived from the Canadian National Topographic Database. The feature points were available with longitude and latitude known. We chose the road intersection points among four types of feature points because they are more easily identifiable in the Ikonos images used. The horizontal accuracy of the CDAL intersection points is specified as 10 m at the 95 percent confidence ellipse (CDAL, 1999), which is approximately equivalent to a 4.1-m root-mean-square error (RMSE). The elevations of the intersection points were derived from the Canadian Digital Elevation Data (CDED) set in the same region. The CDED DEM records elevation values referring to the Canadian Geodetic Vertical Datum of 1928 (CGVD28) orthometric heights, which is different from the WGS84 ellipsoidal heights used for Ikonos imagery. The exact conversion of elevation values between these two geodetic systems was done using GPS-HT, released by the Geodetic Survey Division, Natural Resources Canada. GPS-HT allows GPS, DGPS, and WADGPS users in Canada to convert North American Datum (NAD83) ellipsoidal heights to CGVD28 orthometric heights. The conversion accuracy was estimated as ±5 centimeters with 95 percent confidence in the southern regions of Canada. For each intersection object point, the line (row) and sample (column) coordinates of its corresponding image points in the left and right images were collected, and the image line and sample coordinates were assumed to have a measurement error of 0.3 pixel RMSE.

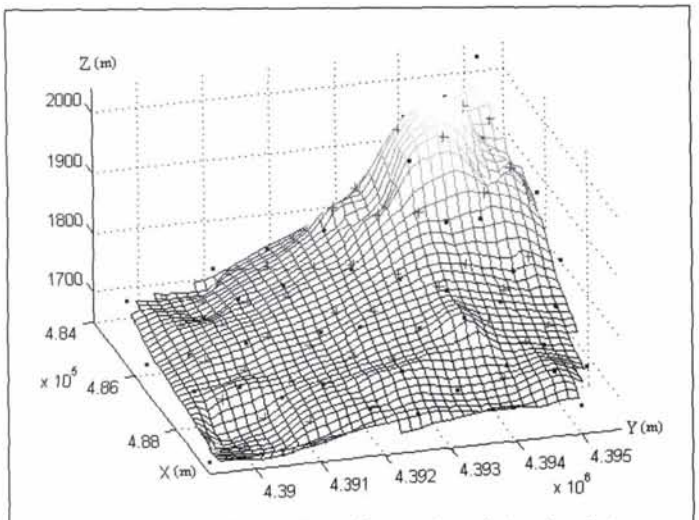

Figure 1. The distribution of control and check points.

Results and Evaluation

Test Case 1

Among the 49 additional points, nine points were selected as additional GCPs, and the other 40 points were used as checkpoints (CKPs). The range in terrain relief for these CKPs is 357.07 meters. To solve for the RFCs, the terrain-dependent approach was used. First, the initial estimates for the RFCs were solved for with the first set of 50 GCPs. Then, both the BILS and IDKF methods were used to obtain the updated RFC estimates. The IDKF method was applied by adding the nine additional GCPs one by one and assigning higher weights to those new GCPs as they were collected from higher resolution imagery. For the purpose of checking the accuracy of the updated solution, we fixed the process noise covariance at $\mathbf{Q} = 10^{-8}$. The 40 CKPs were used to calculate their corresponding positions in the image using the ground-to-image transformation of the RFM (Equation 1) with the new RFC estimates. The Euclidean distance between the calculated positions and the measured positions was used as an indicator for error residuals.

A part of the experiment results is presented in Table 1, showing results computed by the BILS and IDKF methods. The root-mean-square error (RMSE) and the maximum absolute error at CKPs in the image row and column directions are listed. The residual vectors at CKPs for the initial estimate are plotted in Figure 2a. The marks with cross symbol indicate the image positions of the 40 CKPs. The residual vectors at CKPs for the final updated estimate are plotted in Figure 2b. The marks with a small circle indicate the image positions of the nine additional control points. The residual vectors at CKPs from the BILS solu-

TABLE 1. IMAGE ROW AND COLUMN RESIDUALS AT 40 CHECKPOINTS (UNIT: PIXEL)

Number of new GCPs	BILS				IDKF			
	Row		Column		Row		Column	
	RMSE	MAX	RMSE	MAX	RMSE	MAX	RMSE	MAX
0 (initial estimate)	1.134	3.175	0.909	2.700	1.134	3.175	0.909	2.700
1	1.123	3.191	0.909	2.712	1.123	3.205	0.908	2.720
2	1.121	3.253	0.909	2.705	1.258	3.837	0.920	2.945
3	1.122	3.231	0.893	2.575	1.290	3.399	0.863	2.399
4	1.125	3.239	0.893	2.577	1.276	3.322	0.941	2.378
5	1.083	3.238	0.830	2.118	1.241	3.135	0.966	2.399
6	1.078	3.311	0.837	2.175	1.369	3.769	0.857	2.286
7	1.054	3.520	0.842	2.159	1.356	4.315	0.840	2.141
8	0.942	2.950	0.825	2.098	1.274	4.050	0.854	2.177
9 (final estimate)	0.912	3.054	0.824	2.092	1.112	2.827	0.880	2.464

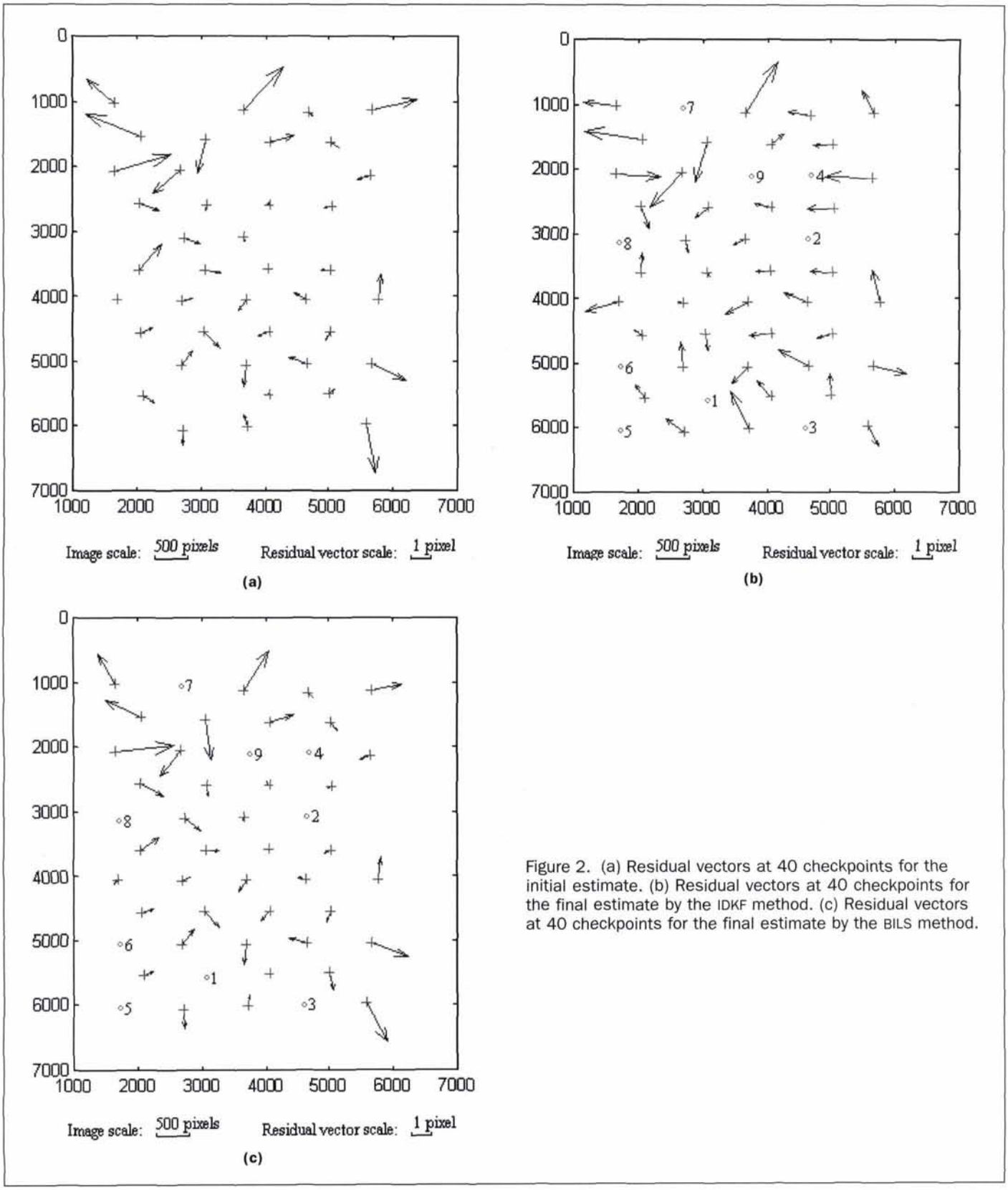

Figure 2. (a) Residual vectors at 40 checkpoints for the initial estimate. (b) Residual vectors at 40 checkpoints for the final estimate by the IDKF method. (c) Residual vectors at 40 checkpoints for the final estimate by the BILS method.

tion for all 59 GCPs are shown in Figure 2c. Figures 3a and 3b delineate the total errors (i.e., the residuals combining row and column directions) at CKPs during the updating process by the BILS and IDKF methods, respectively.

To obtain a single term representing the adjustment accuracy at new GCPs, the average standard deviation is used. It is defined as the root mean of the diagonal elements of the covariance matrix (i.e., Equation 7 for the BILS method and Equation

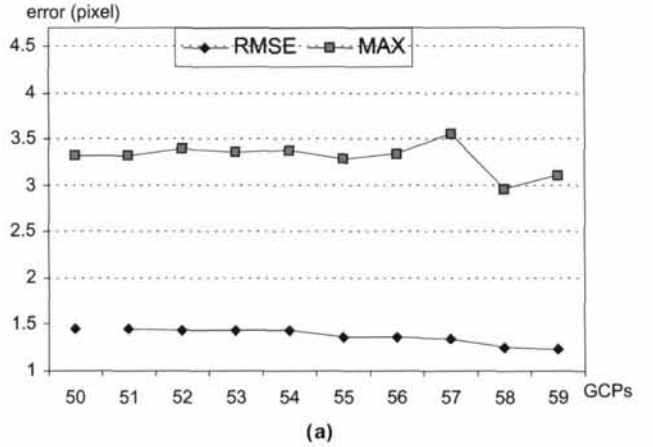

Figure 3. (a) Total errors at 40 checkpoints by the BILS method. (b) Total errors at 40 checkpoints by the IDKF method.

10 for the IDKF method). The computed average standard deviations for the image row and column directions at the new GCPs are listed in Table 2. The first row in Table 2 is the average standard deviation for the initial estimate using the original 50 GCPs.

Before updating, the total RMS error and the maximum absolute error at the CKPs using the 50 GCPs are 1.45 pixels and 3.32 pixels, respectively. For the BILS method after using the 59 GCPs, the total RMS error and the maximum absolute error at the CKPs are 1.23 pixels and 3.10 pixels, respectively. For the final updated solution using the IDKF method, the total RMS error and the maximum absolute error at the CKPs are 1.42 pixels and 2.93 pixels, respectively. An improvement in terms of the final accuracy and the distribution of errors is noticeable after adding nine additional control points.

Table 3. Image Row and Column Residuals at Nine Checkpoints (Unit: Pixel)

Number of new GCPs	BILS				IDKF (groups of five)			
	Row		Column		Row		Column	
	RMSE	MAX	RMSE	MAX	RMSE	MAX	RMSE	MAX
0 (initial estimate)	0.894	1.428	1.151	3.253	0.894	1.428	1.151	3.253
5	0.823	1.931	0.942	2.417	0.668	1.337	1.076	3.047
10	0.757	1.364	0.857	1.552	0.910	1.685	0.913	2.209
15	0.677	1.134	1.059	2.528	0.794	1.875	0.866	2.024
20	0.821	1.824	0.966	2.086	0.646	1.388	0.944	2.170
25	0.627	1.161	0.731	1.585	0.742	1.880	0.786	2.004
30	0.765	1.137	0.951	1.815	0.8115	2.136	0.833	1.925
35	0.442	0.893	0.536	1.146	0.757	1.639	0.679	1.724
40	0.423	0.788	0.579	1.362	0.609	1.098	0.677	1.668

Although the average standard deviations estimated at the new GCPs are smaller than those at the original 50 GCPs (see Table 2), the final estimate is only slightly superior to the initial estimate at the CKPs. This is due to the fact that only nine new GCPs were added to the adjustment. The contribution is not significant compared to the large number of GCPs used to obtain the initial estimate for the RFCs. It is also found that a small number of additional GCPs may not always improve the estimation accuracy at the CKPs (see Figures 3a and 3b).

Test Case 2

Among the 49 points, the nine points selected as additional GCPs in Test Case 1 were used as CKPs in Test Case 2, and the other 40 points were used as additional GCPs. Similar to Test Case 1, the initial estimate of the RFCs was first solved for using the terrain-dependent approach with the 50 GCPs. Then the initial estimate of the RFCs was updated using both the BILS and IDKF methods. For the IDKF method, the results were calculated by adding the additional GCPs one by one and in groups of five points, also assigning a higher weight to those new GCPs.

In Table 3, the RMS and maximum absolute errors at CKPs using both the BILS and IDKF methods with groups of five new GCPs (i.e., five GCPs are assimilated each time) are provided. In Table 4, the average standard deviations at the new GCPs are listed, showing results computed by the BILS method and the IDKF method with new GCPs added one by one and in groups of

Table 2. Average Standard Deviations at Nine New GCPs (Unit: Pixel)

Number of new GCPs	BILS		IDKF	
	Row	Column	Row	Column
0 (initial estimate)	1.001	1.001	1.001	1.001
1	0.408	0.400	0.412	0.410
2	0.406	0.393	0.409	0.405
3	0.404	0.397	0.417	0.420
4	0.399	0.391	0.409	0.411
5	0.401	0.396	0.423	0.423
6	0.402	0.400	0.420	0.421
7	0.404	0.403	0.422	0.423
8	0.405	0.404	0.422	0.420
9	0.402	0.400	0.412	0.415

Table 4. Average Standard Deviations at 40 New GCPs (Unit: Pixel)

Number of new GCPs	BILS		IDKF (one by one)		IDKF (groups of five)	
	Row	Column	Row	Column	Row	Column
0 (initial estimate)	1.001	1.001	1.001	1.001	1.001	1.001
5	0.406	0.406	0.410	0.414	0.410	0.411
10	0.402	0.403	0.416	0.419	0.407	0.408
15	0.392	0.393	0.412	0.411	0.396	0.397
20	0.377	0.380	0.406	0.409	0.381	0.384
25	0.375	0.381	0.424	0.424	0.379	0.384
30	0.375	0.381	0.422	0.422	0.379	0.385
35	0.370	0.374	0.417	0.419	0.373	0.377
40	0.369	0.373	0.412	0.413	0.372	0.376

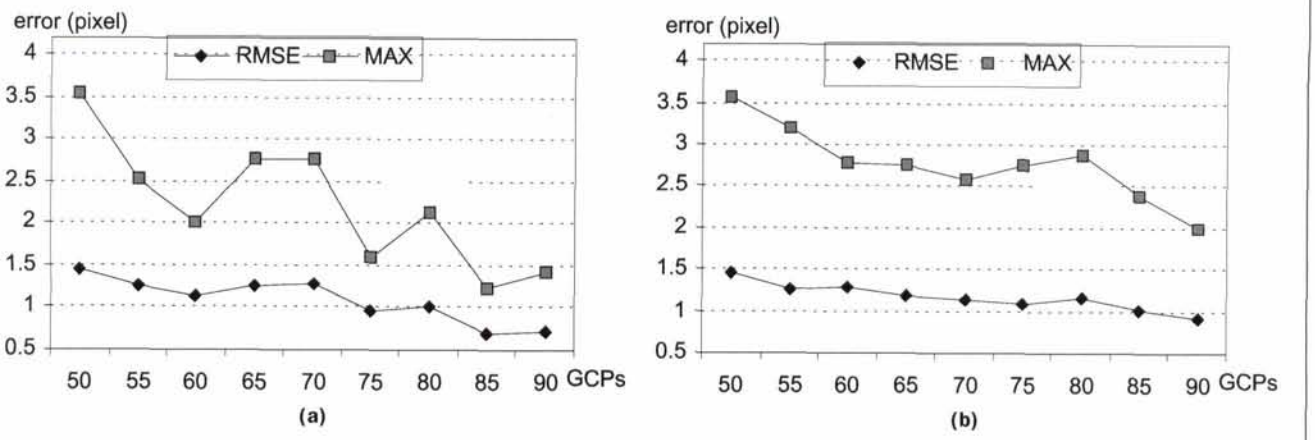

Figure 4. (a) Total errors at 9 checkpoints by the BILS method. (b) Total errors at 9 checkpoints by the IDKF method.

five. Figures 4a and 4b delineate the total errors at CKPs during the updating process by the BILS method and the IDKF method (groups of five), respectively.

The total RMS and maximum absolute errors at the CKPs using the 50 GCPs only reach 1.46 pixels and 3.55 pixels, respectively, before updating. For the BILS method, the total RMS and maximum absolute errors at the CKPs using the 90 GCPs are 0.72 pixel and 1.42 pixels, respectively. For the IDKF method, the total RMS and maximum absolute errors at the CKPs for the final updated solution are 1.17 pixels and 2.44 pixels when adding new GCPs one by one, and 0.91 pixel and 2.00 pixels when adding new GCPs in groups of five. The RMS and maximum absolute errors at the CKPs decrease to about half of the initial estimates. It shows that the accuracy is improved quite significantly when a comparable number of additional GCPs become available.

Test Case 3

The Ikonos stereo-pair data were used in this test. Among the 28 points collected, 20 points were used as additional GCPs, and the remaining eight points were used for accuracy checking purpose. First, we evaluated the accuracy of the RFCs supplied for each image using the eight checkpoints before updating. Then, the 20 GCPs in groups of five were used to update the RFCs pertaining to the left image and right image, respectively, using the IDKF method. Because the covariance associated with the RFCs were not provided, it's assumed to be a zero matrix (i.e., $\mathbf{P} = 0$), and a very small value for the process noise covariance $\mathbf{Q}$ was set to allow for the RFCs updating. The accuracy of the new set of RFCs was evaluated at the eight checkpoints, respectively, for the left and right images. A portion of the results is listed in Table 5. Finally, the RFCs of the stereo pair before and after updating were used to do a 3D reconstruction with the forward rational function model (Di *et al.*, 2001; Tao and Hu, 2001b). The initial ground coordinates were determined by solving the RFM omitting all the second- and third-order terms. The accuracies of the 3D reconstruction results in ground space are compared in Table 6. It shows that the use of the initial RFCs of the Ikonos stereo pair yields a horizontal accuracy of 11.1 m CE90 and a vertical accuracy of 5.6 m LE90. Using the IDKF method with the additional 20 GCPs, the accuracies become 6.1 m CE90 and 3.8 m LE90, respectively, for the second updating. Testing of the Ikonos 3D mapping accuracy is beyond the scope of the paper; interested readers may refer to papers by Baltsavias *et al.*, (2001), Fraser *et al.*, (2001), and Toutin *et al.*, (2001). More detailed descriptions about the 3D reconstruction algorithms using the RFM can be found in Tao and Hu (2001b).

Because the covariance $\mathbf{P}$ associated with the RFCs was not supplied, we let it be zero, and carefully chose a process noise covariance $\mathbf{Q}$. Improvements were achieved when the value of $\mathbf{Q}$ is between 10^{-12} and 10^{-8}. This range is around the magnitude of the smallest value of the RFCs, which is between 10^{-11} and 10^{-10} for the Ikonos stereo pair. However, large values for $\mathbf{Q}$ (e.g., greater than 10^{-8}) will certainly make the second- and third-order terms in the RFM more important. Of course, we can reasonably expect that the updating should be more reliable when $\mathbf{P}$ is provided for Ikonos imagery.

The numerical results listed in Tables 5 and 6 show that both the ground-to-image transformation and the 3D reconstruction are improved after assimilating 20 new GCPs. Although the accuracy of the new GCPs used in this test is limited, the improvement is still satisfactory. This shows that the proposed method can improve the RFCs accompanying the Ikonos standard level stereo products when using additional control points.

Conclusions

When additional control information becomes available, the initial RFM solutions can be updated using the two methods proposed, namely, the BILS and IDKF methods, with the absence of the physical sensor model. The BILS method incorporates all the control points, including those used to calculate the initial estimate of the RFCs, simultaneously into its estimation process, while the IDKF method is applied incrementally when only the new control points are known. It is realized that end-users can expect good results if the covariance matrices for the RFCs and the image measurements can be made available (by the data vendor who calculated the RFM initially).

The accuracy of RFM solutions can be improved using these two methods when a significant number of new GCPs is available. However, they may not result in a better accuracy at checkpoints if the additional control points are not sufficient or the covariance matrices used are not appropriate. The IDKF method is comparable to the BILS method in terms of the accuracy at checkpoints. It was shown that, for discrete Kalman filtering, assimilating groups of several control points is smoother than incorporating only one point at a time. It was also found that assuming a very small but non-zero value for the process noise covariance often leads to better precision at the CKPs in our experiments. This is expected because there are correlations to some extent between the RFCs.

In reality, end users often do not have the control points used by the vendor in calculating the initial estimate of the

TABLE 5. IKONOS IMAGE LINE AND SAMPLE RESIDUALS AT EIGHT CHECKPOINTS (UNIT: PIXELS)

Image	Number of new GCPs	Updating 1 ($\mathbf{Q} = 10^{-10}$)				Updating 2 ($\mathbf{Q} = 10^{-8}$)			
		Line		Sample		Line		Sample	
		RMSE	MAX	RMSE	MAX	RMSE	MAX	RMSE	MAX
Left	0 (initial estimate)	2.391	4.418	6.387	9.839	2.391	4.418	6.387	9.839
	5	2.686	5.164	5.542	8.747	2.271	4.159	4.839	8.469
	10	2.139	4.542	5.063	8.393	2.661	5.864	4.157	7.865
	15	2.356	5.029	4.376	7.593	1.879	4.456	3.204	7.195
	20	2.283	4.764	3.611	6.856	2.038	3.156	3.282	6.968
Right	0 (initial estimate)	2.339	5.038	8.140	10.722	2.339	5.038	8.140	10.722
	5	2.566	5.561	7.250	9.581	2.300	3.361	7.066	9.447
	10	2.077	4.611	6.240	8.434	2.224	5.272	3.754	5.552
	15	2.604	5.859	5.526	7.590	3.762	7.690	3.228	4.847
	20	2.761	6.058	4.533	6.543	2.780	6.105	3.389	5.999

TABLE 6. RMS (MAX.) ERRORS AT EIGHT CHECKPOINTS AFTER 3D RECONSTRUCTION

3D Reconstruction	Easting (meters)		Northing (meters)		Height (meters)		
	RMSE	MAX	RMSE	MAX	RMSE	MAX	MEAN
Initial estimate	3.325	5.924	6.603	9.012	3.383	5.440	−2.694
Updating 1	2.889	5.004	3.607	5.834	2.420	4.149	−1.192
Updating 2	2.318	4.690	3.158	5.278	2.282	4.299	1.023

RFCs. In order to facilitate users to update the RFM solutions using additional control information, it is suggested that the covariance matrix of the RFCs be included in the image transfer meta-data. This helps users to achieve a better updating solution by controlling the system sensitivity to new control information in the Kalman filtering process. Based on the tests using Ikonos images, we can expect a satisfactory refinement using the IDKF method, although the covariance of the RFCs is not provided.

It is worth noting that the incremental technique can also be used as a quality assurance tool to verify the existing estimates using the obtained GCPs of high accuracy, or to determine the quality of new control information relative to the given RFM solutions.

Acknowledgments

The authors wish to thank Mr. Steve Schnick for his great assistance in the Ikonos testing work. We also thank Dr. Bryan Mercer, Intermap Technologies Inc., for providing the aerial photograph data, and Dr. Bob Truong, Canadian Nuclear Safety Commission, for providing the Ikonos images. Special thanks go to Prof. Clive Fraser from the University of Melbourne and Mr. Jacek Grodecki from Space Imaging, for the valuable discussions and helpful comments.

References

Baltsavias, E., M. Pateraki, and L. Zhang, 2001. Radiometric and geometric evaluation of IKONOS Geo Images and their use for 3D building modelling, *Proceedings of Joint ISPRS Workshop "High Resolution Mapping from Space 2001" (CD-ROM)*, 19–21 September, Hannover, Germany, pp. 15–35.

Brown, R.G., and P.Y.C. Hwang, 1997. *Introduction to Random Signal and Applied Kalman Filtering, Third Edition*, John Wiley & Sons, New York, N.Y., pp. 190–241.

CDAL (CGDI Data Alignment Layer), 1999. *Creating the CGDI Data Alignment Layer*, URL: http://cdal.cgdi.gc.ca/html/frames-e.html.

Di, K., R. Ma, and R. Li, 2001. Deriving 3-D shorelines from high resolution IKONOS satellite images with rational functions, *Proceedings of 2001 ASPRS Annual Convention* (CD ROM), 23–27 April, St. Louis, Missouri, unpaginated.

Dowman, I., and J.T. Dolloff, 2000. An evaluation of rational functions for photogrammetric restitution, *Int. Arch. Photogrammetry and Remote Sensing*, 33(Part B3):254–266.

Fraser, C.S., H.B. Hanley, and T. Yamakawa, 2001. Sub-meter geopositioning with IKONOS geo imagery, *Proceedings of Joint ISPRS Workshop "High Resolution Mapping from Space 2001" (CD-ROM)*, 19–21 September, Hannover, Germany, pp. 61–68.

Greve, C.W., C.W. Molander, and D.K. Gordon, 1992. Image processing on open systems, *Photogrammetric Engineering & Remote Sensing*, 58(1):85–89.

Grodecki, J., and G. Dial, 2001. IKONOS geometric accuracy, *Proceedings of Joint ISPRS Workshop "High Resolution Mapping from Space 2001" (CD-ROM)*, 19–21 September, Hannover, Germany, pp. 77–86.

Krakiwsky, E.J., 1990. *The Methods of Least Squares: A Synthesis of Advances*, UCGE Reports 10003 Department of Geomatics Engineering, University of Calgary, Calgary, Alberta, Canada, 21 p.

Madani, M., 1999. Real-time sensor-independent positioning by rational functions, *Proceedings of ISPRS Workshop on Direct versus Indirect Methods of Sensor Orientation*, 25–26 November, Barcelona, Spain, pp. 64–75.

Newman, D.J., 1978. *Approximation with Rational Functions*, Regional Conference Series in Mathematics No. 41, American Mathematical Society, Providence, Rhode Island, 52 p.

OpenGIS Consortium, 1999. *The OpenGIS Abstract Specification - Topic 7: Earth Imagery*, URL: http://www.opengis.org/techno/abstract/99-107.pdf.

Paderes, F.C., Jr., E.M. Mikhail, and J.A. Fagerman, 1989. Batch and on-line evaluation of stereo SPOT imagery, *Proceedings of the ASPRS-ACSM Convention*, 02–07 April, Baltimore, Maryland, pp. 31–40.

Tao, C.V., and Y. Hu, 2001a. The rational function model - A tool for processing high-resolution imagery, *Earth Observation Magazine*, 10(1):13–16.

———, 2001b. 3-D reconstruction algorithms with the rational function model and their applications for IKONOS stereo imagery, *Proceedings of Joint ISPRS Workshop "High Resolution Mapping from Space 2001"* (CD-ROM), 19–21 September, Hannover, Germany, pp. 252–263.

———, 2001c. A comprehensive study of the rational function model for photogrammetric processing, *Photogrammetric Engineering & Remote Sensing*, 67(12):1347–1357.

———, 2001d. Use of the rational function model for image rectification, *Canadian Journal of Remote Sensing*, 27(6):593–602.

Toutin, T., and P. Cheng, 2000. Demystification of IKONOS, *Earth Observation Magazine*, 9(7):17–21.

Toutin, T., R. Chénier, and Y. Carbonneau, 2001. 3D Geometric Modelling of IKONOS Geo Images, *Proceedings of Joint ISPRS Workshop "High Resolution Mapping from Space 2001"* (CD-ROM), 19–21 September, Hannover, Germany, pp. 273–281.

Yang, X., 2000. Accuracy of rational function approximation in photogrammetry, *Proceedings of the ASPRS Convention* (CD-ROM), 22–26 May, Washington, D.C., unpaginated.

(Received 21 August 2001; accepted 16 November 2001; revised 15 December 2001)